Available online at www.sciencedirect.com

ScienceDirect

Procedia CIRP 44 (2016) 245 – 250

www.elsevier.com/locate/procedia

6th CIRP Conference on Assembly Technologies and Systems (CATS)

Simulation and design of an orientation mechanism for assembly systems

Daniel Krebs[a], Gunnar Borchert[a]*, Annika Raatz[a]

[a]*Leibniz Universität Hannover, Institute of Assembly Technology, 30823 Garbsen, Germany*

* Corresponding author. Tel.: +49-511-762-18245 ; fax: +49-511-762-18251. *E-mail address:* borchert@match.uni-hannover.de

Abstract

The article focuses on methods for designing modular cable-driven orientation mechanisms that can be attached to robot systems that lack on rotational degrees of freedom. The approach yields assembly systems for high speed handling applications by reducing moving masses. For this purpose, a classification of feasible kinematic structures are given and resulting characteristics, like the orientation workspace, dexterity or its homogeneity, are analyzed. The mechanical design of a first prototype is subsequently presented along with a universal simulation tool for determining task-adapted powertrains using cables. Finally, results of first tests and possibilities for future developments are presented.

Peer-review under responsibility of the organizing committee of the 6th CIRP Conference on Assembly Technologies and Systems (CATS)

Keywords: assembly robot; parallel kinematic; orientation mechanism; cable-driven

1. Introduction

The article is concerned with the improvement of the mobility of robot systems for handling and assembly which are based on *Clavel*'s delta structure [1]. The delta structure is widely used to achieve translational motion for pick and place operations (PPO) at very high speeds. However, various issues, such as changes in the product design could necessitate the need for a higher number or different types of degrees of freedom (DoF). In light of this situation, current systems in academic and industrial research are augmented with an additional rotational axis to achieve *Schoenflies* motions. An example thereof is provided in [2, 3], where an additional motor is attached to the mobile platform of a delta structure. Other approaches are demonstrated given the examples of M-1iA and M-3iA by *Fanuc Robotics* [4, 5] or FlexPicker by *ABB Robotics* [6]. The first robot has three rotational DoF, realized through revolute joints that are serially attached to the mobile platform, where the motors are fixed to the base and connected by telescopic shafts and universal joints. In contrast, M-3iA has the motors attached to the parallelogram arms of the delta structure. FlexPicker has only one rotational DoF, with the motor fixed to the base and a telescopic shaft as powertrain. These examples illustrate that additional axes require additional motors or powertrains, the integration of which into the basic robot system (target system) becomes a challenge and which must be considered precisely. High performance motors and robust powertrains are needed to achieve the short cycle-times typically required for PPO. However, this generally comes with high inertias, which impairs the performance of the target system and increases the cycle-time. Further considerations of possible robot designs with additional orientation axes are presented in [7] along with analyses that account for the impact of different extension mechanisms on the dynamics of a delta structure.

This article presents a modular orientation device (MOD) which is actuated by means of Bowden control cables (Bcc). This design allows to integrate additional rotational DoF while reducing the inertia effects on the robot. The motors are fixed to the base and thus decoupled as far as possible from the moving robot system. The weight of the powertrain and therefore the mechanical stress on the structure of the target system is much lower. Such an approach is proposed in [8]. In general, its use does not depend on the design of the actuated mechanism, which is why no kinematic structures are presented. Still, different structures exist and, according to *Schopen* [9], adaption of the kinematic structure to the desired task should be done. To limit the number of possible solutions, the work presented here focuses on spherical mechanisms with three rotational axes (RRR). As stated by *Siciliano* et al. [10], spherical RRR mechanisms in particular provide the highest dexterity. Moreover, the position can be decoupled from the

Peer-review under responsibility of the organizing committee of the 6th CIRP Conference on Assembly Technologies and Systems (CATS)
doi:10.1016/j.procir.2016.02.122

orientation of the MOD [11], which supports the desired modular mechanical and control design. Other advantages are the simple mechanical design, the absence of interfering contours or a simple cable handling [12]. Since different spherical RRR structures are possible, the article first introduces a formalism of suitable configurations. Each of them yields different characteristics of the MOD, such as homogeneity or dexterity because of which the orientation workspace should be analyzed. Workspace analysis is a common topic in research: In [13] different parameterization methods are investigated, for example a method based on Euler-angles. Here, various global performance measures are implemented so that the quality of the orientation workspace can be evaluated. In doing so, the orientation workspace volume is constituted as equi-volumetric elements. Further research that either considers the measurement of the workspace volume or uses the latter as an objective performance measure to optimize the design of manipulators can be found in [14, 15]. Other performance measures such as dexterity, or condition indices e.g. the Global Dexterity Index (GDI) or the Workspace Index (WI) can be found in [16, 17, 18]. Another analysis is shown in [19], where a classification of RRR manipulators is presented based on the topology of the workspace. After evaluating the orientation workspace, this article presents the mechanical design of a first prototype along with a universal tool for designing task-adapted powertrains with Bcc. Finally, results of a first test and possibilities for future developments are presented.

2. Structural characteristic of the RRR mechanism

As defined by *Schopen* [9], three serially combined joints are necessary to provide a workspace with maximum orientation. To this end, each joint must be revolute with one DoF, where the axes of adjacent joints are typically parallel or orthogonal (crossing angles: 0° or 90°). Other crossing angles are possible but are neglected for simplification. The notation is defined as: rotations about *x*, *y* and *z* become A, B and C. Moreover, the revolute joints are subdivided in axially aligned and not axially aligned with respect to their axes of rotation.

In reference to [9], 27 possible configurations arise from the variation of all joint axes. However, they can be reduced to 12 by taking their joint arrangement into account. This is due to the fact that configurations are not reasonable for providing a full orientation when two adjacent joints are parallel to each other [9]. Those joint configurations are redundant, i.e. singular. As a result of this, we neglect parallel axes of adjacent joints and obtain two sets of six configurations where either the first and third axes of a configuration are parallel or all three axes are orthogonal. So far, each configuration provides a maximal redundant orientation workspace due to unlimited joint angles and infinite resolution. By considering mechanical interferences of adjacent links, the angular range of not axially aligned joints will be restricted to ±100° (initial assumption). Further assumptions are that two configurations can be transferred into each other, if and only if C-joints are used. This rule is applied to avoid mechanical reconfigurations. That means the initial shape of the MOD, as shown in Fig. 1, should be kept as it is. In detail, the end-effector should point in *z*-direction and the links should all be vertically aligned. The second requirement entails that C-joints must be axially aligned, whereas A- and B-joints do not align. An overview on the remaining independent configurations is given in Fig. 1.

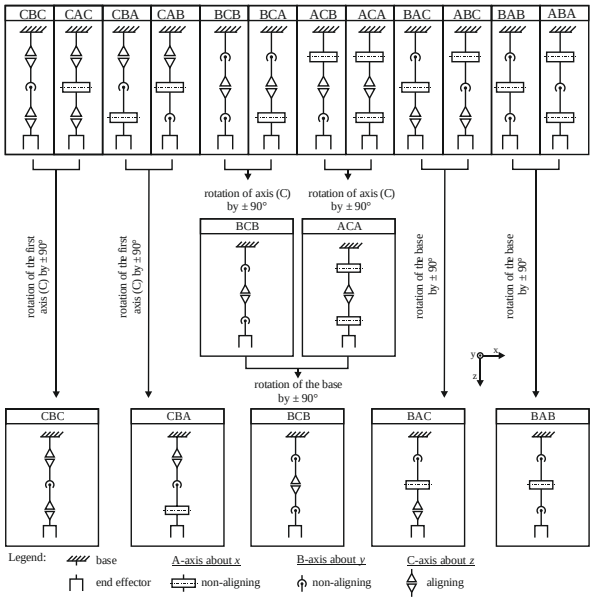

Fig. 1. Development of suitable RRR configurations.

2.1. Inverse kinematics: attainable orientation workspace

For orientation workspace analysis, a finite partition of the workspace is done. As shown in Fig. 2, a normal vector ${}^0z_{E,i}$ is used that forms a grid on a sphere with the resolution of ΔC. The rotation of ${}^0z_{E,i}$ will then complete the (so far unrestricted) orientation workspace. The inverse kinematics are then used to solve for possible configurations for the restricted case. The results are shown in Fig. 3. Black areas have no solutions. Within the cyan area redundant configurations are attainable. A green area depicts a full orientation, i.e. exact one possible configuration. The color gradation, in turn, depicts the number of possible rotational steps $0 < j < 360$ about ${}^0z_{E,i}$. It becomes obvious that the orientation of the CBC structure is limited to ±100°, however, it provides redundancy and a full orientation characteristic for the remaining orientation workspace. Redundant configurations can occasionally be found for BAC,

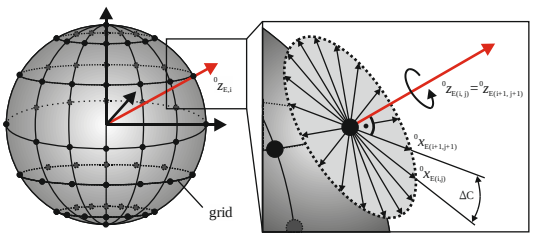

Fig. 2. Numerical interpretation of the orientation workspace

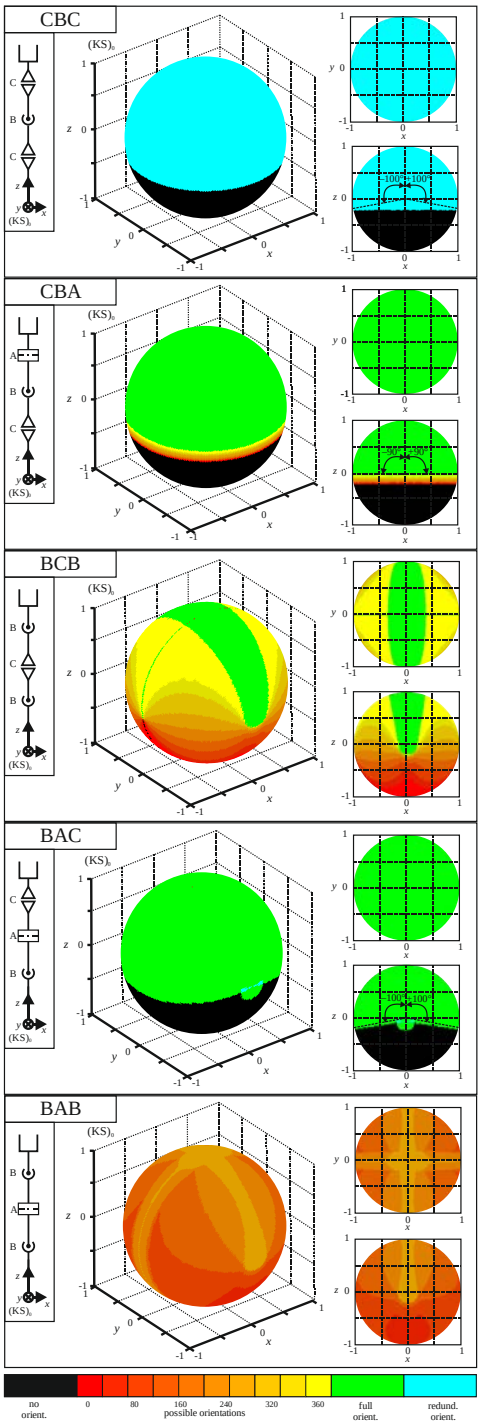

Fig. 3. Orientation workspace of different RRR configurations.

too. However, the full orientation characteristic is predominant. It also applies to CBA within an orientation range of ±90°. This is followed by small transition with limited orientation of up to 10° towards the area beyond the attainable orientation workspace. Such areas cannot be seen within the orientation workspace of BCB and BAB. The normal vectors ${}^0z_{E,i}$ of both can be varied without any restrictions. Nevertheless, its rotation is then partly limited. In particular, regarding the BAB structure which has no configurations with a full orientation.

2.2. Jacobi matrix: dexterity

The Jacobian J is used to consider the dexterity index of serial robotic manipulators which is based on the condition number $\kappa(J) = \|J\|\cdot\|J^{-1}\|$, with $\kappa(J) \geq 1$, where $\|\cdot\|$ is any norm of the matrix. Here $\|\cdot\|$ is the weighted *Frobenius* norm which is defined as $\|J\| = \mathrm{sqrt}(J\cdot W\cdot J^T)$, with $W = (1/n)\cdot I$ [17]. I denotes the identity matrix and n the dimension of J. As described in [17], the reciprocal $1/\kappa(J)$ is the local conditioning index (LCI) which gives some indication of the local property of the MOD. This is why the LCI is just partly meaningful for comparing the entire orientation workspace among the MOD. For this purpose, the LCI can be transformed into the global conditioning index (GCI) $\eta = A/B$, with $A = \int_O(1/\kappa)\mathrm{d}O$ and $B = \int_O \mathrm{d}O$, as demonstrated by *Kucuk* et al. [18]. O denotes an orientation within the workspace and B the volume of the latter. The GCI ranges from 0 (J is ill-conditioned) to 1 (J is well-conditioned). The GCI of the analyzed MOD are summarized in Tab. 1. The highest GCI (most promising MOD with respect to dexterity) is provided by the BAB configuration followed by BAC and CBC. The lowest GCI can be found with CBA.

Table 1. GCI calculation for different RRR configurations.

	CBC	CBA	BCB	BAC	BAB
GCI	0.3634	0.2785	0.3009	0.3714	0.3892

2.3. Direct kinematics: homogeneity

In order to analyze the influence of the resolution of rotary encoders on the attainability of the orientation workspace, the direct kinematics for discrete rotational steps is solved. A sphere represents the orientation workspace (see Fig. 4) and the area elements A_i of the grid are considered instead. The direct kinematics are then used to compute the number of possible orientations within each area element, i.e. how many vectors ${}^0z_E$ are inside A_i. The total number of orientations are normalized with respect to the corresponding A_i. The results are depicted in Fig. 5. The counts per element are shown using colored bars. It should be mentioned that a different scale is used for CBC. Red colored spots indicate regions with a high number of possible orientations, while blue spots represent a lower number. This representation gives indeed no information on ${}^0x_E$ or ${}^0y_E$ so that ${}^0z_E$ must then be put in

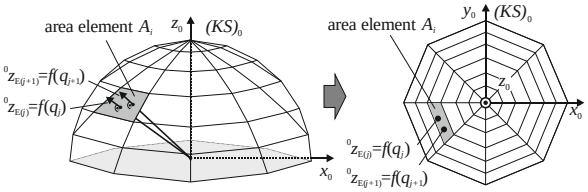

Fig. 4. Partition of the orientation workspace for homogeneity analysis.

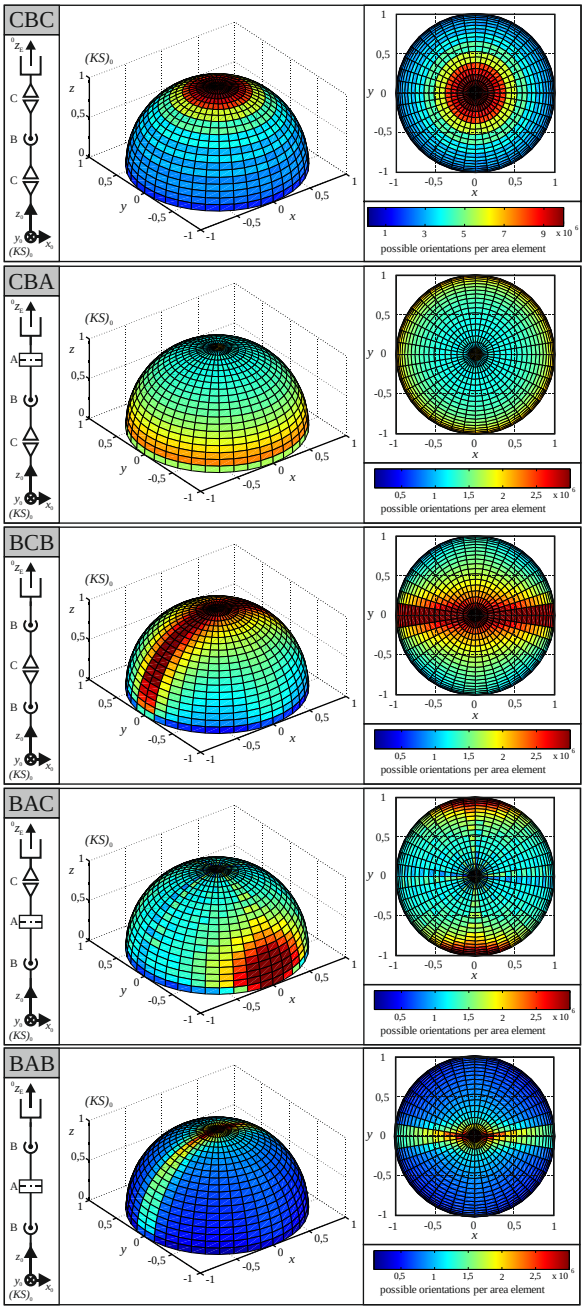

Fig. 5. Homogeneity of the orientation workspace of different RRR configurations and representation of singularities.

relation with the results of Sec. 2.1. Nevertheless, it is useful to investigate if possible orientations are evenly distributed within the orientation workspace or not. This type of distribution is considered as ‘homogeneity’ in the following. It becomes obvious that none of the structures has a homogenous orientation workspace as a result of singularities. The representation of singularities is another interesting outcome. Since the *Jacobian* is rank-deficient when the first and third axis are aligned, singularities of Type 1 [20] are present. In general, due to prioritizing techniques when solving the inverse kinematics (decoupling of the first and third joint), the structure can generate more orientations for, respectively near such areas. In conclusion, structure CBC provides an outstanding high number of possible orientations compared to the others using the same encoder resolution. A reason for this can be found with the redundant behavior (cf. Sec. 2.1 or Fig. 3)

2.4. Results of the orientation workspace analysis

Based on the results, it can be concluded that the CBC configuration shows advantageous characteristics compared to the other structures. CBC has the largest orientation workspace by considering a full orientation characteristic (cf. Fig. 3). By using the same encoder resolution, it also provides the highest number of possible orientations (cf. Fig. 5). The most promising structure with respect to dexterity is BAB followed by BAC. Nevertheless, the GCI of CBC is in the same range (cf. Tab. 1) so that it shows the best overall performance when taking the restricted orientation workspace into account.

3. Design and test of the first prototype

As a result of Sec. 2, the first prototype is finally based on a CBC structure. The mechanical design of the MOD is shown in Fig. 6 along with the drive unit for each axis.

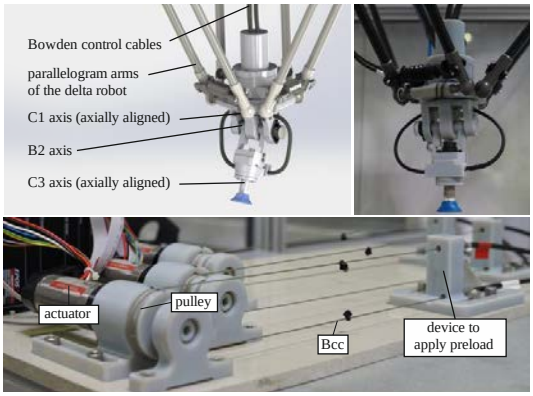

Fig. 6. CAD design (left) and first prototype of the CBC MOD (right) with decoupled motors and Bowden control cables (bottom).

3.1. Mechanical design

Two main aspects for designing cable-controlled MODs can be highlighted: the dynamic performance of the target system and the integration of the Bcc. With respect to the target system, its dynamic performance must not be impaired by the MOD. For this reason, the MOD design features low masses, like small sensors, which yields low moments of inertia of the axes. Moreover, the center of gravity of the entire MOD is close to the center of the mobile platform to avoid forces and moments due to acceleration of the target system.In addition to the dynamic performance, the manner of integrating the Bcc into the MOD is crucial for the final motion characteristic of the latter. To provide positive and negative motions, q_{pos} and q_{neg}, i. e. a bidirectional motion, two complementary Bcc are

used for each axis (cf. Fig. 7, pair of green/red cables). Both Bcc of an axis move relative to their previous axis and thus represent an interference contour so that a safe and collision-free operation between the Bcc and the MOD must be guaranteed. They are thus guided inside the structure of the MOD. The interference contour of the cables is reduced so that the orientation workspace will not be restricted.

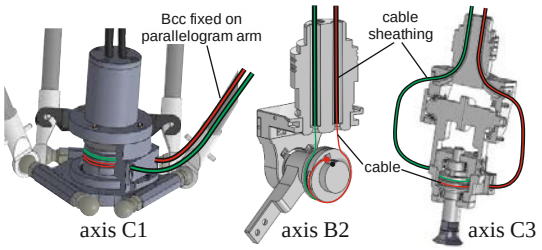

Fig. 7. Structural guided Bcc; axes C1 (left), B2 (middle) and C3 (right)

3.2. Powertrain design tool

A design tool was developed for determining a task-dependent drive unit which is based on Bcc. A key feature of the tool is that jerk and angular acceleration of the MOD axes (with respect to the input and output of the powertrain) can be calculated depending on the needed and the maximum torque allowed.

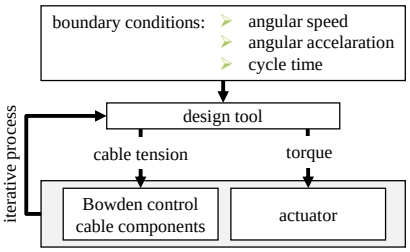

Fig. 8. Flowchart of the iterative design tool

The tool is based on a jerk limited trajectory. It is used for determining the resultant load at the MOD structure due to accelerations. The boundary conditions for the trajectory are derived from a reference (90-400-90) mm PPO for delta robots [21] with a cycle time of 0.75 s. Other important parameters are: angular range, rotational speed, acceleration and jerk. It is required that the MOD passes through the angular range within the specified cycle time. Thus, the range of the angular path is defined by the unrestricted motion of the joints: ±100° for B-joints and ±180° for C-joints, see Sec. 2. The maximal angular speed of the axes can be calculated by taking the nominal speed of the actuator and the transmission ratios of the gear box and pulley of the Bcc into account. Due to the encoder resolution, the transmission ratio of the pulley affects the angular accuracy and speed of the joints of the MOD, as shown in Fig. 9.

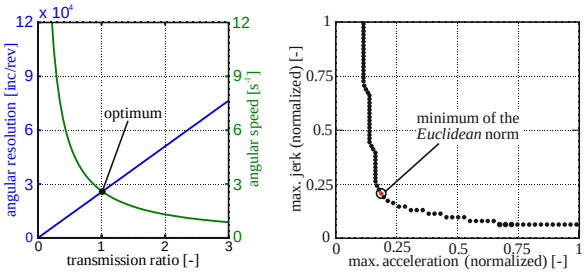

Fig. 9. Influence of the transmission ratio on angular resolution and angular speed (left) and the set of valid parameter combinations a_{motor} and j_{motor} (right)

For the given application with high dynamic but also precise movements, the velocity and the accuracy should be as high as possible. As depicted in Fig. 9 (left) the maximal value of both parameters can be found at the transmission ratio 1:1 of the pulley. Moreover, mechanical stress at the MOD should be reduced so that the needed acceleration and jerk must be as low as possible. For this purpose, the jerk time is varied for the path planning algorithm to calculate a set of valid combinations of the acceleration a_{motor} and jerk j_{motor} (cf. Fig. 9, right). To make a selection, the acceleration and the jerk in Fig. 9 are normalized. The optimally combined values are then defined by the minimum of the *Euclidean* norm.

The maximal joint torques can be determined by considering a worst case load scenario for each axis as demonstrated in Fig. 10. The maximal torques M_{C1}, M_{B2}, M_{C3} are a result of the maximum acceleration of the MOD and the target system (a_{TS}~100 m/s²) as well as the gravity force g in combination with the moments of inertia of the axes J_{C1}, J_{B2}, J_{C3} and the payload J_{Load}, and the masses m_{C1}, m_{B2}, m_{C3} and m_{Load}. Based on these calculations the needed maximal actuator torque and the maximal cable tension can be evaluated by using the transmission ratio of the pulley. The torque is used to check if the actuator meets the requirement. The cable tension will then define the components of the Bcc. Otherwise, the input parameters of the design process, like the underlying actuator characteristics, needs to be adjusted iteratively. The combination of a_{motor} and j_{motor} can alternatively be varied.

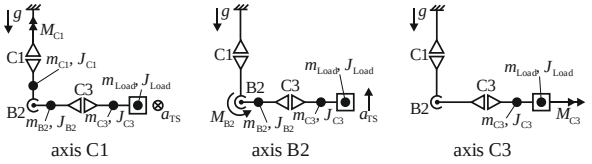

Fig.10. Worst case load scenario; axes C1 (left), B2 (middle) and C3 (right)

3.3. Testing

A sample application with open-loop control, i.e. a sinusoidal signal, was applied to illustrate the influence of the elasticity of the Bcc on the performance of the MOD. The comparison between the desired and the measured angles are shown in Fig. 11. Basically, two characteristics can be illustrated in Fig. 11: ① backlash and ② a direction dependent inaccuracy of the attainable angle.

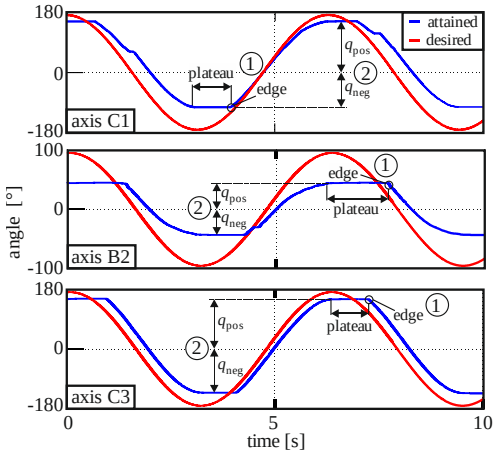

Fig. 11. Results of a first test with sinusoidal input signal for each axis

① The attained profile of the angle has a *plateau* where the rotational direction changes. The orientation remains unchanged until the backlash due to the elastical and frictional characteristic of the Bowden cables is overcome. The motion will then start abruptly, which is marked as *edge* in Fig. 11.

② Another consequence of the flexibility of the Bcc is that the desired angles can not be attained (without feedback control). The deviations Δq of the measured maximal angles q_{pos} and q_{neg} are summarized in Tab. 2. The differences between Δq_{pos} and Δq_{neg} are caused by the mechanical set-up, which makes it difficult to adjust the preload of the cables. It should be mentioned that the deviations of axis B2 are much higher compared to the other axes. This is caused by bending forces of the cables of axis C3 (see Fig. 7, right).

Future work could be a feedback control to overcome the disadvantageous characteristics of the flexible Bcc.

Table 2. Comparison of the measured angles attained during the first test (-) represents a desired value

	measured angle [°]		**deviation [%]**	
axis	q_{pos}	q_{neg}	Δq_{pos}	Δq_{neg}
C1	160.3 (180)	-109.4 (-180)	10.9	39.2
B2	44.1 (100)	-48.0 (-100)	55.9	52.0
C3	159.1 (180)	-148.3 (-180)	11.6	20.9

4. Conclusions

The contribution is concerned with the development of a modular cable-driven RRR mechanism which could be used to extend the motion functionality of a conventional industrial delta robot. To this end, investigations of the structural synthesis of RRR mechanisms are presented along with the analysis of the orientation workspace. In doing so, performance measures, like homogeneity or dexterity, are introduced and the results are discussed. In the end, a spherical CBC wrist structure was chosen to be designed. The first prototype and its mechanical design are then presented. In addition, a tool for designing the powertrain, which is based on Bowden control cables, is shown. Finally, results of a first test with open-loop control are presented to illustrate the influence of the Bowden control cables on the performance of the mechanism.

References

[1] Clavel R. (1988). Delta: a Fast Robot with Parallel Geometry, In: Proceedings of the 18th Int. Symposium on Industrial Robot, Lausanne.
[2] Omron Europe B.V. Delta Robots Datasheet, Online available via: https://industrial.omron.eu/en/products/catalogue/motion_and_drives/robots/delta_robots/delta_robots/default.html [cited on 26.11.15].
[3] KOCH Pack-Systeme GmbH. Customized machine technology, Brochure, Online available via: http://www.koch-pac-systeme.com/uploads/media/KOCH_Machine_broschure_EN_06.pdf [cited on 27.11.15].
[4] Fanuc Robotics America Corporation. Datasheet: FANUC Robot M-1iA. FRA-6/9/2014, Online available via: http://www.fanucrobotics.com/cmsmedia/datasheets/M-1iA%20Series_171.pdf [cited on 14.07.15].
[5] Fanuc Robotics America Corporation. Datasheet: FANUC Robot M-3iA. FRA-24/02/2014, Online available via: http://www.fanucrobotics.com/cmsmedia/datasheets/M-3iA%20Series_168.pdf [cited on 14.07.15].
[6] ABB AG. Datasheet: IRB360 FlexPickerTM Industrieroboter. Ver.ROB0082 EN_G Dec2013, Online available via: http://new.abb.com/products/robotics/industrial-robots/irb-360 [cited on 14.07.15].
[7] Borchert, G., Raatz, A., 2015, An Analysis Process to Improve the Mobility of a Parallel Robot for Assembly Tasks, 14th World Congress in Mechanism and Machine Science, 25-30 October, Taipei, Taiwan.
[8] Binder J., Pott A. and Schäfer J. (2012) Drive system for driving e.g. delta robot in food industry, has Bowden cables arranged between driving apparatus and joint, where force is exerted on joint through cables for movement of joint with degree of freedom of driving apparatus, Patent DE 102011101206 A1, published 15. Nov. 2012.
[9] Schopen M. (1986). Die Auswahl von Handhabungsgeräten aufgrund der charakteristischen Merkmale ihrer kinematischen Strukturen, VDI Fortschrittberichte, Reihe 2: Fertigungstechnik Nr. 127, VDI Verlag.
[10] Siciliano B., Sciavicco L., Villani L. and Oriolo, G. (2009). Robotics, Modelling, Planning and Control, Springer.
[11] Pieper D.L. (1968). The kinematics of manipulators under computer control, Ph.D. thesis, Dept. of Computer Science, Stanford University.
[12] Hesse S. and Malisa V. (2010). Taschenbuch Robotik, Montage, Handhabung, Karl Hanser Verlag München, ISBN 978-3-446-41969-8.
[13] Guilin Yang et. al (2006). Numerical Orientation Workspace Analysis with Different Parameterization Methods, IEEE Conference on Robotics, Automation and Mechatronics 2006, Bangkok, pp. 1-6.
[14] Chen C. and Jackson D. (2011). Parameterization and Evaluation of Robotic Orientation Workspace: A Geometric Treatment, IEEE Transactions on Robotics, Vol. 27, Issue 4, pp. 656 – 663.
[15] Panda S., Mishra D. and Biswal B.B. (2009). An appropriate tool for optimizing the workspace of 3R robot manipulator, In: Proc. of World Congress on Nature & Biologically Inspired Computing, pp. 1156-1161.
[16] Babu K. and Rao K. (2014). Orientation Workspace Analysis of a 3-DoF Planar Parallel Kinematic Machine, In: Int. Journal of research in mechanical engineering technology (IJRMET), Vol. 4, Issue 2, pp. 168-172.
[17] Angeles J. and López-Cajún C.S. (1992). Kinematic Isotropy and the Conditioning Index of Serial Robotic Manipulators, International Journal of Robotics Research, Vol. 11, No. 6, pp. 560–571.
[18] Kucuk S. and Bingul Z. (2006). Comparative study of performance indices for fundamental robot manipulators, Robotics and Autonomous Systems 54 (2006), Vol. 54, Issue 7, pp. 567–573.
[19] Baili M., Wenger P. and; Chablat D. (2004). A classification of 3R orthogonal manipulators by the topology of their workspace, In: Proc. IEEE Int. Conf. on Robotics and Automation, Vol. 2, pp. 1933–1938.
[20] Gosselin C.M. and Angeles J. (1990) Singularity analysis of closed-loop kinematic chains, IEEE Transactions on Robotics and Automation, Vol. 6, No. 11, pp. 281-290.
[21] Borchert G., Battistelli M., Runge G. and Raatz A. (2015) Analysis of the mass distribution of a functionally extended delta robot, In: Robotics and Computer-Integrated Manufacturing, Vol. 31, February 2015, pp. 111-120.